Available online at www.sciencedirect.com
ScienceDirect
Trans. Nonferrous Met. Soc. China 22(2012) 2139−2145
Transactions of Nonferrous Metals Society of China
www.tnmsc.cn

Effects of Ce in novel bronze and its plasma sprayed coating

LI Wen-sheng[1], LIU Yi[1], WANG Zhi-ping[1], MA Chao[2], WANG Shun-cai[2]

1. State Key Laboratory of Advanced Nonferrous Materials, Lanzhou University of Technology, Lanzhou 730050, China;
2. National Centre for Advanced Tribology, School of Engineering Sciences, University of Southampton, Southampton SO17 1BJ, UK

Received 7 September 2011; accepted 10 January 2012

Abstract: A novel aluminum bronze over the Cu−Al binary alloy eutectoid Cu−14Al−4.5Fe was prepared by a jointly-charging one-melting technique and conventional sand casting. The bronze coatings were atmospherically plasma sprayed on the 45# medium carbon steel substrate. The effect of rare earth Ce on the microstructures and Vickers hardness of the cast alloy and coatings were characterized by scanning electron microscopy, X-ray diffraction, electronic probe microanalysis, transmission electron microscopy and microhardness measurements. The results indicate that the hardness of both as-cast alloy and coating are enhanced by the addition of 0.6% Ce due to the refinement of κ phases which are well distributed in the matrix. The rapid solidification in the plasma spray processing retains Fe-supersaturated in the Al-bronze alloy coatings, which avoids the formation of eutectoid ($\alpha+\gamma_2$) phase and stacking faults are found in the coatings with Ce added, accordingly improves the mechanical properties.
Key words: rare earth; Ce; aluminum bronze; plasma spraying coating

1 Introduction

Aluminum bronze alloy has low shear strength in nature, good tribological properties and high strength, which is comparable to mild steel [1]. A novel aluminum bronze has been developed for precision stainless steel and thin ferrous sheet forming dies [2,3], with the Al content over the Cu−Al binary alloy eutectoid of about 14%. However, the equilibrium solubility of Al in bronzes is less than 9.4%, conventional sand casting techniques are not feasible to fabricate high aluminum bronze because of foundry complications associated with the narrow range of solidification and the eutectoid reaction that occurs at 565 °C (which results in the β phase breaking down to $\alpha+\gamma_2$ phases) [4,5]. This eutectic reaction can cause embitterment and is especially likely to occur at low cooling rates [6]. To achieve high rates of cooling and thus to avoid the formation of γ_2 phase, a low-pressure atmospheric plasma spraying technique is employed. This technique gives very high rates of cooling because of the high droplet velocity and small droplet size of the molten powder [7,8].

With strong chemical activities and rather large atomic radius, rare earths (RE) can react easily with many elements such as H, O, N, S and Si, and play a favorable role in molten metals refining and successfully have been applied to modify the Mo/Ni/Co baized surface properties of the thermal spray coatings, thermal spray welding coatings and laser alloyed coatings [7−10]. There is an increasing interest in understanding the rapid solidification, particle re-melting and precipitation, interface transformation, interface moving effect, counter flow pattern, alloying reaction and the relationship between microstructures and properties of surface modified layers [11,12]. RE in the as-casts bronze has been studied but less in bronze coatings.

In this study, an attempt of rare earth Ce element addition was made to assess the potential of Ce in the aluminum bronze and its coatings synthesized by low-pressure atmospheric plasma on a medium steel substrate. The effects of Ce on the microstructures and Vickers hardness were also studied.

Foundation item: Projects (50804019, 51165021) supported by the National Natural Science Foundation of China; Project (0901ZTB009) supported by the Super Tutor Foundation from the Education Department of Gansu Province, China
Corresponding author: LI Wen-sheng; Tel: +86-931-2976640; Fax: +86-931-2975037; E-mail: wensheng-li@sohu.com
DOI: 10.1016/S1003-6326(11)61440-4

2 Experimental

2.1 Materials

The chemical composition of the novel bronze is listed in Table 1. The specimen was prepared by jointly-charging one-melting technique [2,13]. The as-received metals are of electrolytic purity ≥99.95%.

Table 1 Chemical composition of Cu−14Al−4.5Fe alloy (mass fraction, %)

Cu	Al	Fe	Co	Ni	Others
80	13	3.0	0.8	0.6	2.6

In the preparation process, Cu and Al were placed into a furnace. The other metals Co, Ni, Fe and Mn were then mixed into the copper and aluminum pieces. Furthermore, about 5% Al (part of the 13% Al in the composition of the alloy as listed in Table 1) was left as pre-deoxygenating and temperature-tuning reagents. The furnace was pre-heated for 5 to 8 min at a low heating rate in order to exclude the oil and gas, and then a higher heating rate was used to melt all the raw materials as quickly as possible. After all the raw materials were completely melted, a layer of charcoal with a thickness of 20−30 mm was used to cover the molten surface. During the processing, inert gas of nitrogen or argon was used. Then, a process of pre-deoxygenating was carried out using the residual of about 5% Al. Meanwhile, the melting temperature was adjusted to 1200−1260 °C. A chemical refining was then performed using C_2Cl_6 and/or C_2Cl_4 refining reagents with an amount of 0.1% to 0.15% of all the molten materials. Following that, an eventual deoxygenating process was taken using rare earth (Ce). Before pouring, a gas check was done to ensure the Chinese standard GB/T 1176−1987. Finally, the melted materials were poured into sand moulds at 1180−1240 °C or gas atomized by nitrogen with cool water.

2.2 Processing of coating

In order to assess the effect of rare earth addition to plasma sprayed components, the samples of Cu−14Al−4.5Fe bronze coatings with and without 0.6% Ce were prepared and deposited under the same conditions. The powders of Cu−14Al−4.5Fe−Ni alloy were produced by gas atomization in a nitrogen atmosphere with cool water. The pre-alloy was prepared by a jointly charging one-melting technique.

The coating was deposited with a plasma gun. The schematic diagram of the device is shown in Fig. 1. A high voltage (about 120 kV) between the tungsten cathode and the copper anode ionized the plasma gas to form the plasma flame. The current for the plasma formation was 170 A. The bronze powder is fed via the exit point of the flame from the aperture of the device (feed rate of 60−120 g/min). The molten droplets formed after being accelerated by the plasma gas. They stroke the surface of the substrate and formed thin platelets that conformed, adhered and interlocked with each other and with the substrate surface [8,9,14] to build up a coating layer up to thickness of 0.8−2.0 mm. The deposited material was gas-atomized powder with an average diameter of 70−145 μm and the gun-substrate distance was 50−100 mm. The coated material was cooled down naturally.

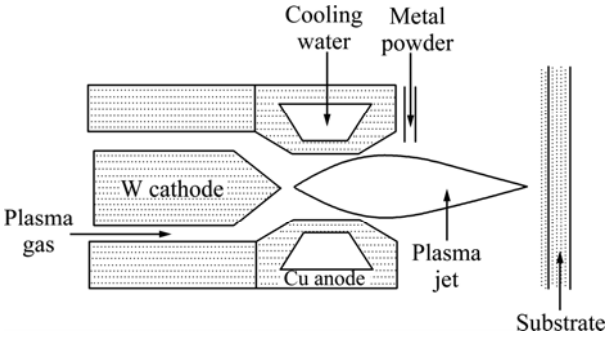

Fig. 1 Schematic diagram of low-pressure plasma spraying gun

2.3 Microstructure analysis and hardness test

The micro-hardness of as-cast alloy and coatings was determined by a Vickers microhardness tester (Shimadzu Micro-hardness Tester Type M) under a load of 0.98 N. A JEM 6700F scanning electron microscope (SEM) was used. Micro-analysis and chemical mapping were performed by an EPMA−1610 electronic probe microanalysis (EPMA) equipped with an OXFORD ISIS 300 EDS analyzer. A D/MAX2500PC diffractometer was used with Cu K_α (λ=1.54186 Å) radiation at a scanning rate of 0.02(°)/s and step of 5 s. Transmission electron microscopy was used for structure determination.

The specimens for optical, SEM and EPMA observations were etched using a solution consisting of 5 g $FeCl_3$, 10 mL HCl and 100 mL distilled water (CS solution). A solution containing 5 g $(NH_4)_2SO_4$, 10 g citric acid, 30 mL H_3PO_4 and 1000 mL distilled water (SS solution) was used for identifying the κ phases. The TEM specimens were prepared using electro-polishing solution of 20% HNO_3, 15% 2-butoxyethanol and 65% methanol, and observed at 300 kV.

3 Results

3.1 Microstructures of as-cast alloy and coatings

The optical microscope images of the as-cast Cu−14Al−4.5Fe without and with 0.6 % Ce addition are presented in Fig. 2. The microstructures are characterized by grey grains, white matrix phase and dot-like dark

phases. Furthermore, the dot-like dark phases (Fig. 2 (b)) in Cu−14Al−4.5Fe bronze with 0.6% Ce addition are more refined and homogeneously distributed than those without Ce addition (Fig. 2 (a)).

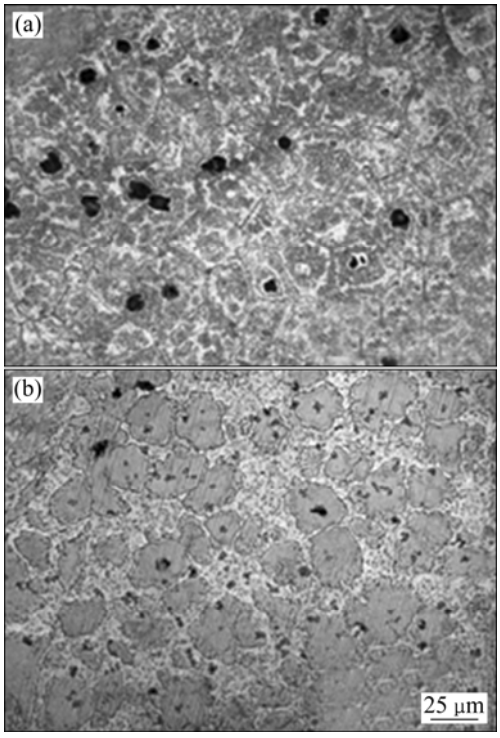

Fig. 2 Optical metallographs of Cu−14Al−4.5Fe bronzes: (a) Without Ce; (b) With 0.6% Ce addition

Figure 3(a) shows the SEM backscattered electron image of the as-cast Cu−14Al−4.5Fe bronze with 0.6% Ce addition which was electrolytic alloy etched in the SS solution. The dot-like dark phases in Fig. 2(b) are presented in a stereo-dimensional appearance. Figure 3(b) shows the SEM image of as-cast Cu−14Al−4.5Fe bronze with 0.6% Ce addition, which was etched in the CS solution. When the Vickers microhardness tester indenter moved across, a scratched trace is left on the surface, except for a break point on the dot-like dark phases, as shown in Fig. 2(b). It reveals that the dot-like dark phases are harder and stronger than the matrix.

The microstructures of the plasma sprayed coatings of Cu−14Al−4.5Fe bronze with and without 0.6% Ce addition are shown in Figs. 4(a) and (b), respectively. It reveals that the bronze coatings with 0.6% Ce addition have finer crystals with an approximately spherical/ rod-like appearance. In contrast, the Cu−14Al−4.5Fe bronze coating without Ce addition consists of dendrites with high aspect ratio similar to the typical thermal spray coating.

The XRD patterns of the Cu−14Al−4.5Fe bronze with 0.6%Ce addition of as-cast alloy and plasma sprayed coating are presented in Fig. 5. The peaks are consistent with the ones from β', α, γ_2 and κ phases. The

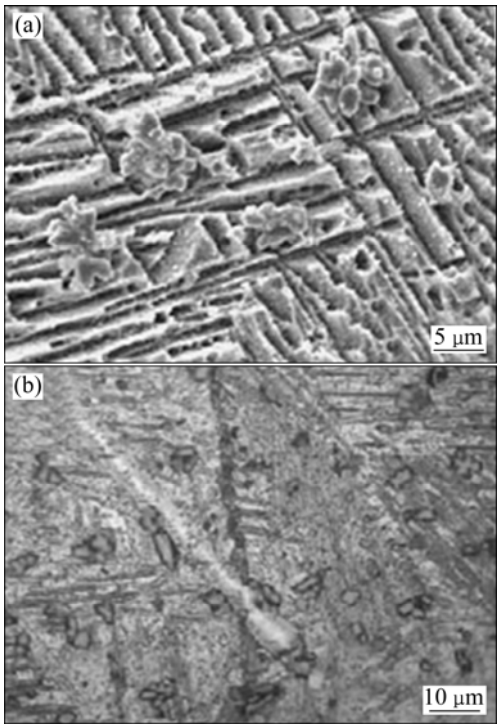

Fig. 3 SEM images of Cu−14Al−4.5Fe bronze with 0.6% Ce addition: (a) Electrolytically etched in SS solution; (b) Etched in CS solution

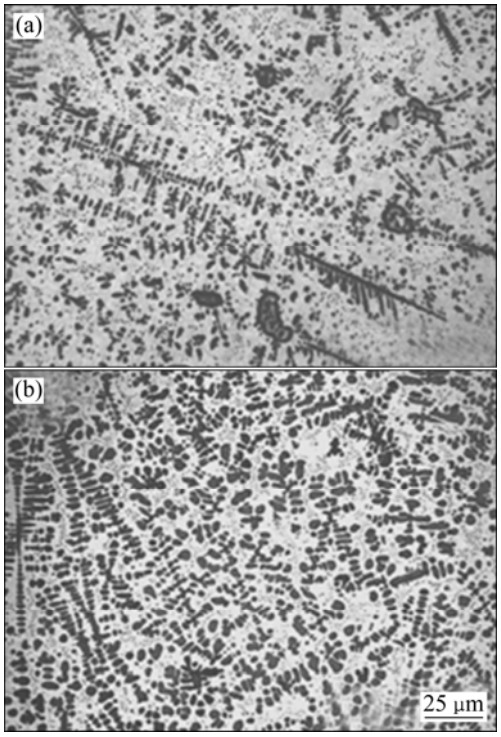

Fig. 4 Optical metallographs of aluminum bronze coatings: (a) Without Ce; (b) With 0.6% Ce addition

as-cast alloys have a complex phase combined with β', α, γ_2 and κ_2. In contrast, the plasma sprayed coatings are dominated by two phases of β' and κ_1. The difference is

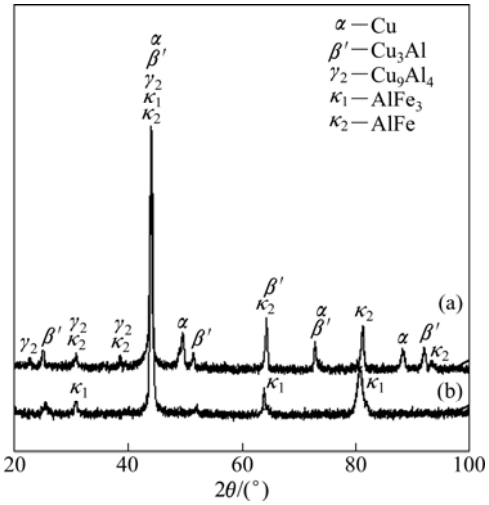

Fig. 5 XRD patterns of with 0.6% Ce: (a) As-cast; (b) Coating of Cu−14Al−4.5Fe bronze

considered to be caused by the different cooling rates. The characteristics of the equilibrium phases in aluminum bronze alloy are listed in Table 2 [2,6].

The EDS results [2,3] showed that the grey phases in the microstructure of Cu−14Al−4.5Fe as-cast bronze are retained β or β' phase and α phase with a micro-composition of 9.35% Al, 1.01% Fe, 0.64% Mn, 0.08% Co and 88.1% Cu, etc, and have a micro-hardness of HV 264. The light areas are most likely eutectoid (α+γ_2) phases, with a composition of 9.52% Al, 0.7% Fe, 0.58% Mn, 0.19% Co and 87.6% Cu, etc, and a micro-hardness of HV 314. The fine dot-like dark phases dispersed in the alloys are the intermetallic κ_2 phases, with a micro-hardness of HV 413.

Different from the microstructures of Cu−14Al−4.5Fe as-cast bronze, the microstructures of the coating (Figs. 4(a) and (b)) are composed of grey β' and Fe

Table 2 Characteristics of equilibrium phases in aluminum bronze

Phase	Description	Crystal structure	Lattice spacing/nm	Hardness (HV)
α	Copper-rich solid solution	A1	0.364	200−270
γ_2	Intermetallic compound Cu_9Al_4 with wide solubility range	$D8_3$	0.869	360−570
β'	Intermetallic compound Cu_3Al with wide solubility range	L12	0.353	290−407
κ_1	Intermetallic compound $AlFe_3$	DO_3	0.571	>700
κ_2	Intermetallic compound AlFe	B2	0.29	>413

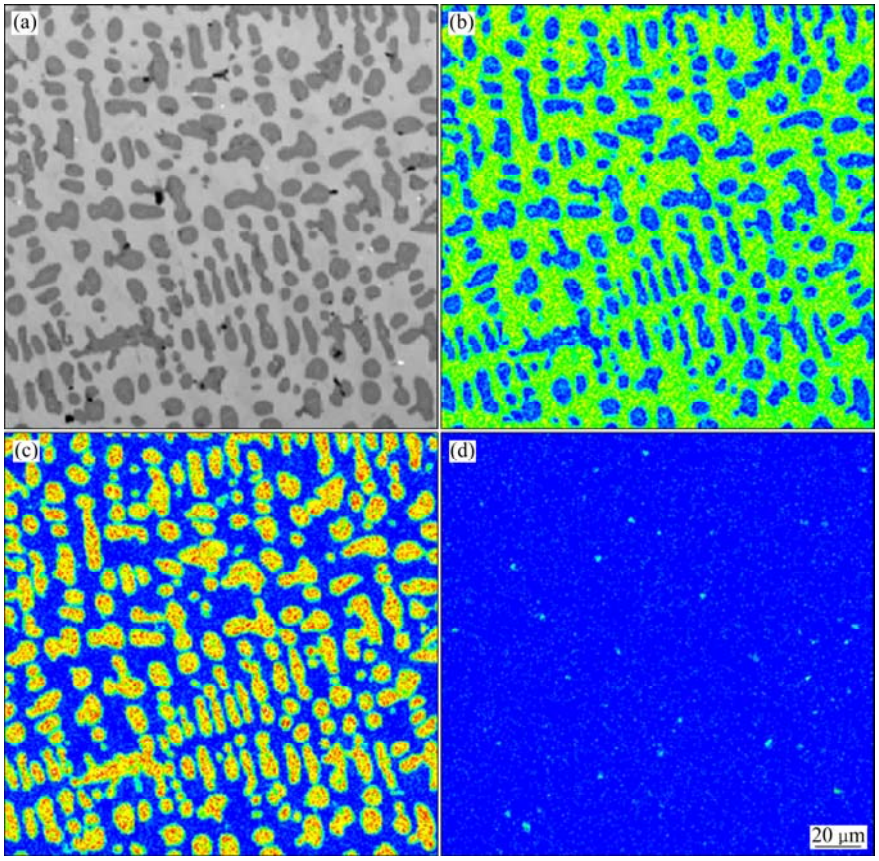

Fig. 6 Second electron image of Cu−14Al−4.5Fe coating (a) and element maps of Cu (b), Fe (c) and Ce (d)

enriched intermetallic κ_1 phases, with hardness of HV 289 and 440, respectively. The EDS mapping shown in Fig. 6 on coating clearly shows a Cu rich matrix and a Fe rich phase, which corresponds to β' phase (Cu_3Al) and κ_1 ($AlFe_3$) phase.

3.2 Ce in as-cast alloy and coatings

Figure 7(a) presents an EPMA high-resolution backscattered electron image of the as-cast aluminum bronze with 0.6% Ce addition, which was electrolytically etched by SS solution to enhance the existence of Ce. The EDS analysis of Fig. 7(a) shows Ce (white point) appears along the grain boundaries. Figure 7(b) presents the EPMA electron image of the coating with 0.6% Ce addition. Ce (white point) is found along the boundaries of the κ_1 ($AlFe_3$) phase, as shown in Fig. 6, the shape of which is influenced by Ce [12]. The compositional profile in Fig. 8 also shows the existence of lead and oxygen, in the possible form of Ce oxides and PbCe compound [11,12].

Figure 9 shows the TEM images of Ce-added coating. Stacking faults are clearly seen, which contributes to the strengthening [15].

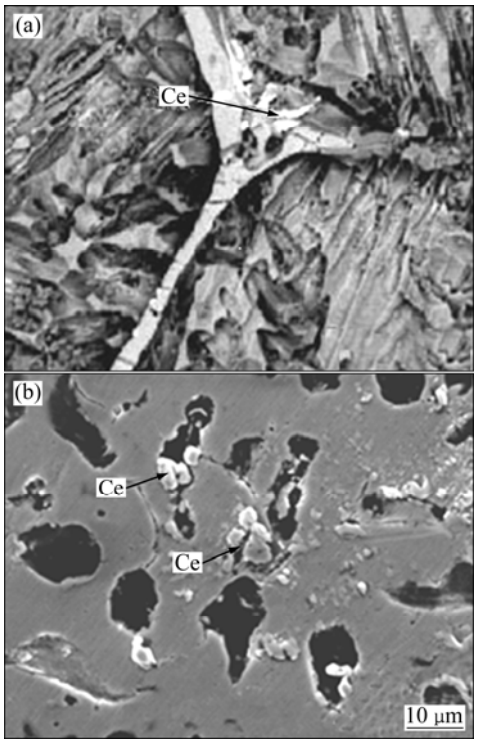

Fig. 7 EPMA backscattered electron images of Cu−14Al−4.5Fe bronze with 0.6% Ce addition and its coating: (a) As-cast alloy electrolytically etched in SS solution; (b) Coatings etched in CS solution

3.3 Hardness

The mechanical properties of the as-casts and coatings are presented in Table 3. It can be seen that the hardnesses of the as-cast alloy and coating with 0.6 % Ce addition increase by 4% and 9%, respectively, compared to those without Ce addition. The plasma sprayed bronze coatings possess higher hardness than the as-cast alloy. Therefore, it can be concluded that the coating with Ce addition has the best hardness, which would have the best wear resistance.

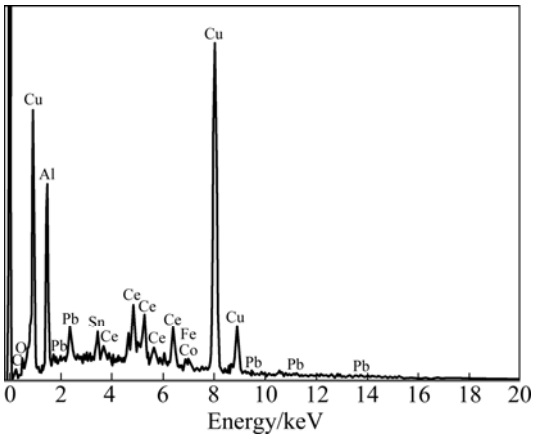

Fig. 8 EDS analysis result of grain boundary

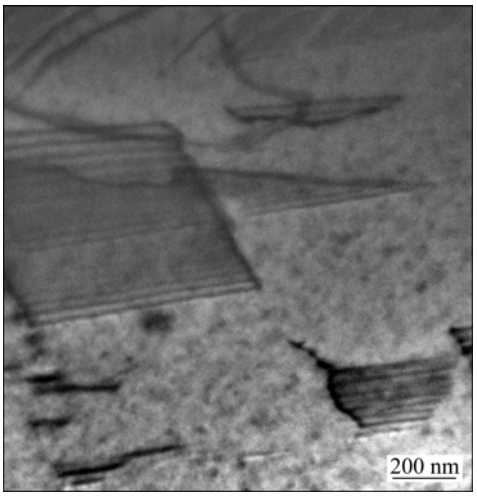

Fig. 9 TEM images of Ce-added coating

Table 3 Hardness of Cu−14Al−4.5Fe bronze of as-cast alloy and coating

Hardness (HV)	With 0.6% Ce addition				Without Ce			
	1	2	3	Average	1	2	3	Average
As-cast	294	290	281	288	284	266	279	276
Coating	321	332	325	326	297	305	289	297

4 Discussion

4.1 Effects of plasma spraying process on coatings

In plasma spraying process, the Cu−14Al−4.5Fe powder begins to melt when the temperature reaches its melting point of 1085 °C. As the temperature further

increases, the liquid infiltrates the substrate surface and then wets and completely covers the substrate surface [9,10]. A high cooling rate is achieved for plasma spray because of its droplet velocity and small droplet size. The formation of the eutectoid ($\alpha+\gamma_2$) phase is avoided, compared to the slow cooling rate for the as-casts where the eutectoid ($\alpha+\gamma_2$) phase exists [2,6] in addition to β' and κ_1 phases, as indicated in Fig. 5.

4.2 Effects of Ce on microstructures of as-cast alloy and coating

As shown in Figs. 2(a) and (b) and Figs. 4(a) and (b), κ phases with 0.6% Ce addition tend to be round shape. In contrast, the coating without Ce addition appears to be dendrite with high aspect ratio of needle-like grains that are commonly seen in the typical thermal sprayed coating. In the as-cast alloy without Ce addition, κ phase appears to be coarse and uniform. Those are due to the refining effects of Ce to the as-cast alloy and powder atomization pre-alloy [11,16].

As there is a lot of oxygen in the molten Cu−14Al−4.5Fe metal, CeO_2 is formed when Ce is added [11,12,16]. CeO_2 has a dual effect on either the nucleation during as-cast solidification and/or the inhibition of grain growth during spraying. The nucleating effects make the powder spherical and uniformly distributed. The melting point of CeO_2 is about 2500 °C, therefore CeO_2 particles are not melted during the spraying process and can act as heterogeneous nucleation sites for the crystal nucleation during solidification. This will increase the grain density in the coating, as shown in Fig. 6(d). Ce fits well to the distribution of the dark κ phases in Fig. 6(a). In addition, during the growth of the nucleated grains, CeO_2 particles are pushed by the solid/liquid interface to the grain boundaries as observed in metal matrix composites [12,16], as shown in Figs. 7(a) and (b). Ce can also purify the oxygen in molten metal. On the other hand, the segregated CeO_2 along the grain boundaries tends to hinder further grain growth by pinning the grain boundaries [11,12]. As a result, the as-cast alloy and coatings are refined and strengthened. This also accounts for the differences in the coarse needle-like microstructures as observed in Fig. 4(a) and the large number of small spherical/rod-like κ_1 phase as shown in Fig. 4(b).

4.3 Hardness of as-cast alloy and coating

Because the cooling time of the deposited particles is very short, a high rate of cooling is achieved after plasma spraying, and the formation of the eutectoid ($\alpha+\gamma_2$) phase in aluminum bronze is avoided. Coatings are composed of β' matrix and the Fe enriched intermetallic κ_1 phase, which exhibit a higher hardness than the as-cast alloy with a microstructure consisting of α, β', γ_2 and κ_2 phases, since α phase is softer than β phase (as listed in Table 2) and the eutectoid ($\alpha+\gamma_2$) phase is brittle in nature.

The difference between the hardness of the two coatings might be due to the fact that the average grain size in Cu−14Al−4.5Fe bronze coating with 0.6% Ce addition is smaller than that in Cu−14Al−4.5Fe bronze coating without Ce as shown in Fig. 4.

5 Conclusions

1) The plasma spray deposition process possesses a rapid solidification to prevent the formation of the eutectoid ($\alpha+\gamma_2$) phase in aluminum bronze. The coatings are mainly composed of β' phase matrix and Fe enriched intermetallic κ_1 phase, which results in a higher hardness.

2) As the increase of heterogeneous nucleation site for crystal nucleation during solidification, the as-cast alloy and coating with 0.6% Ce addition exhibit refined κ phases which are well distributed in the matrix. The stacking faults are found in the coatings with Ce addition, which contributes to the strengthening.

References

[1] HEIDE E V, STAMA E D, GIRAUD H, LOVATO G, AKDUT N, CLARYSSE F, CAENEN P, HEIKILL I. Wear of aluminium bronze in sliding contact with lubricated stainless steel sheet material [J]. Wear, 2006, 261(1): 68−73.

[2] LI W S, WANG Z P, LU Y, JIN Y H, WANG F. Mechanical and tribological properties of a novel aluminum bronze material for drawing dies [J]. Wear, 2006, 261(2): 155−163.

[3] LI Wen-sheng, WANG Zhi-ping, LU Yang, GAO Yong, XU Jian-lin. Preparation, mechanical properties and wear behaviours of a novel aluminum bronze for dies [J]. Transactions of Nonferrous Metals Society of China, 2006, 16(3): 607−612.

[4] JAMES E, KRZANOWSKI J E. Characterization of Fe-supersaturated Fe−Al bronze coatings fabricated by magnetron sputter deposition [J]. Materials Characterization, 1995, 35(4): 207−212.

[5] YASAR M, ALTUNPAK Y. The effect of aging heat treatment on the sliding wear behavior of Cu−Al−Fe alloys [J]. Materials & Design, 2009, 30(3): 878−884.

[6] KAPLANA M, YILDIZ A K. The effects of production methods on the microstructures and mechanical properties of aluminum bronze [J]. Materials Letters, 2003, 57(28): 4402−4411.

[7] PISTOFIDIS N, VOURLIAS G, PAVLIDOU E, PATSALAS P, STERGIOUDIS G, POLYCHRONIADIS E K. Study of the structure and morphology of plasma-sprayed tin coating [J]. Surface and Coatings Technology, 2006, 200 (22−23): 6245−6250.

[8] HWANG B, LEE S, AHN J. Correlation of microstructure and wear resistance of molybdenum blend coatings fabricated by atmospheric plasma spraying [J]. Materials Science and Engineering A, 2004, 366(1): 152−163.

[9] ALAM S, SASAKI S, SHIMURA H. Friction and wear characteristics of aluminum bronze coatings on steel substrates sprayed by a low pressure plasma technique [J]. Wear, 2001, 248(1−2): 75−81.

[10] ZHANG Zhong-li, LI De-yuan, WANG Shui-yong. High temperature performance of arc-sprayed aluminum bronze coatings for steel [J]. Transactions of Nonferrous Metals Society of China, 2006, 16(4): 868−872.

[11] ZHANG Zhen-yu, WANG Zhi-ping, LIANG Bu-nv. Effect of CeO_2 on microstructure and bond strength of Fe−Ni−Cr alloy [J]. Journal of Rare Earths, 2005, 23(1): 73−76.

[12] ZHAO Tao, CAI Xun, WANG Shun-xing, ZHENG Shi-an. Effect of CeO_2 on microstructure and corrosive wear behavior of laser-cladded Ni/WC coating [J]. Thin Solid Films, 2000, 379(1/2): 128−132.

[13] LI Wen-sheng, WANG Zhi-ping, LU Yang, YUAN Li-huang. Corrosive wear behavior of Al-bronzes in 3.5% NaCl solution [J]. Journal of Materials Engineering and Performance, 2006, 15(1): 102−110.

[14] LI Wen-sheng, LU Yang, YANG Xiao-tian, ZHAO Xu-dong, LI Ya-fei, WANG Ya-qing. Structure and property of high aluminum bronze coating sprayed with plasma melt coating [J]. Journal of Lanzhou University of Technology, 2009, 35(3): 4−9. (in Chinese)

[15] LI Wen-sheng, LU Yang, YUAN Ke-xiang, YUAN Chong-guang. Effects of cerium on microstructure and bonding strength of Cu−14Al−4.5Fe bronze plasma sprayed coating [J]. Journal of Rare Earths, 2011, 29(4): 363−369.

[16] WANG You, KOVACEVIC R, LIU Jia-jun. Mechanism of surface modification of CeO_2 in laser remelted alloy spray coatings [J]. Wear, 1998, 221(1): 47−53.

新型铝青铜及其喷涂层中 Ce 元素的作用

李文生[1]，刘 毅[1]，王智平[1]，马 超[2]，王顺才[2]

1. 兰州理工大学 材料科学与工程学院 有色金属新材料国家重点实验室，兰州 730050，中国；
2. 南安普顿大学 工程学院 国家先进摩擦学中心，南安普顿 SO17 1BJ，英国

摘 要：采用一次共装熔炼、砂型铸造 Al 含量超过 Cu−Al 二元合金共析点的新型铝青铜合金 Cu−14Al−4.5Fe，在 45#中碳钢表面制备铝青铜等离子喷涂层。通过扫面电镜、X 射线衍射分析、电子探针、透射电镜和显微硬度计分析 Ce 元素对新型铝青铜合金及喷涂层表面组织形貌和维氏硬度的影响。结果表明：添加 0.6% Ce 到铸态合金及喷涂层可以使细化的 κ 相均匀分布于基体，并提高材料硬度。等离子喷涂层快速凝固，保留铝青铜涂层中 Fe 元素的过饱和固溶体，避免生成(α+γ_2)共析相。含 Ce 喷涂层中的堆垛层错是提高材料力学性能的因素。

关键词：稀土；铈；铝青铜；等离子喷涂层

(Edited by FANG Jing-hua)